Check for updates

Plasma Processes and Polymers

PLASMA PROCESSES AND POLYMERS

RESEARCH ARTICLE

Investigating the Influence of the Substrate Temperature and the Organic Precursor on the Mechanical Properties of Low-Pressure Plasma Polymer Films

Robin Dantinne[1] | Nathan Vinx[1] | Philippe Leclère[2] | Damien Cossement[3] | Claude Poleunis[4] | Arnaud Delcorte[4] | Rony Snyders[1,3] | Damien Thiry[1]

[1]Chimie des Interactions Plasma-Surface (ChIPS), CIRMAP, University of Mons, Belgium | [2]Laboratory for Physics of Nanomaterials and Energy (LPNE), Research, Institute for Materials Science and Engineering, CIRMAP, University of Mons, Belgium | [3]Materia Nova Research Center, Mons, Belgium | [4]Institute of Condensed Matter and Nanosciences (IMCN), Université catholique de Louvain (UCL), Louvain-la-Neuve, Belgium

Correspondence: Damien Thiry (Damien.Thiry@umons.ac.be)

Received: 13 July 2024 | **Revised:** 23 August 2024 | **Accepted:** 28 August 2024

Funding: This research was supported by the French Community of Belgium ("Communauté française de Belgique") through a FRIA grant.

Keywords: growth mechanism | low-pressure discharge | mechanical and viscoelastic properties | plasma polymerization | substrate temperature

ABSTRACT

This work aims to investigate the influence of the substrate temperature on low-pressure plasma polymerization processes. Emphasis is placed on the mechanical properties and growth mechanism of the plasma polymer films (PPFs). For this purpose, two precursors are considered, differing only by their unsaturation degree: 2-propen-1-ol (CH_2=CH–CH_2–OH) and propan-1-ol (CH_3–CH_2–CH_2–OH). Although propan-1-ol-based PPFs behave like hard elastic solids, 2-propen-1-ol-based coatings evolve from a liquid film to an elastic solid on increasing the substrate temperature. This behavior is understood considering the evolution of the glass transition temperature of PPFs. The latter is correlated with the cross-linking degree of the polymeric network governed by the energy density of bombarding ions on the growing film.

1 | Introduction

Studied for several decades, the plasma polymerization method has emerged as a promising technique for the synthesis of tailor-made organic thin films due to the outstanding properties of the layers, including good thermal stability, insolubility in most solvents, and excellent adhesion properties on almost all kinds of substrates. Moreover, the absence of a solvent and the industrial scalability of the method justify the popularity of the plasma polymerization technique [1–3].

Briefly, an organic molecule, called a "precursor," is vaporized in a deposition chamber and activated in a plasma. Reactive species, including radicals and to a lesser extent ions, are formed by electron-induced collisions and condensate on surfaces exposed to the plasma, resulting in the formation of a solid organic thin film referred to as a plasma polymer film (PPF) [4]. Due to the complex interplay between the surface and gas-phase reactions, this material presents many differences from conventional polymers, such as the absence of repeating units in the film, and for most of the synthesis conditions, a highly cross-linked polymeric network is formed.

Depending on the chemical nature of the organic precursor, PPFs can have specific chemical functions (e.g., –SH [5], –NH_2 [6], –OH [7], –Br [8], etc.) of interest for various applications

Abbreviations: **allyl-PPF$_{X°C}$**, PPF synthesized with allyl alcohol at a substrate temperature "X"°C; PCA, Principal Component Analysis; PF-QNM, Peak-Force Quantitative Nanomechanical Mapping; PPF, plasma polymer film; prop-PPF$_{X°C}$, PPF synthesized with allyl alcohol at a substrate temperature "X"°C; ToF-SIMS, time of flight-secondary ions mass spectrometry; T_S, substrate temperature; T_T, surface transition temperature; XPS, X-ray photoelectron spectroscopy.

© 2024 Wiley-VCH GmbH.

such as immobilization of nanoparticles [9] or biomolecules [10], control of cellular growth [11], or fabrication of biosensors [12]. The performance of the functionalized PPFs in such applications requires fine control of their chemical composition. In this context, it appears quickly obvious that the need for a PPF with a precise chemical composition requires a deeper understanding of the relationship between the process parameters and PPF properties [13]. Considerable efforts have therefore been made in the past to elucidate the growth mechanism of functionalized PPFs at a molecular level mainly as a function of the energy load in the plasma.

Because of the high density of radicals compared to the ions, the former were often expected to drive the PPF growth through reaction with molecules or other radicals [4, 14, 15]. Highlighting the peculiarities of the plasma polymerization process, Yasuda proposed the concept of "atomic polymerization" (as opposed to conventional "molecular polymerization"), where, for a high power dissipated in the plasma, the PPF is formed by the recombination of small fragments and atoms derived from the fragmentation of the precursor molecules [16]. Yasuda further developed his model considering the "Rapid Step-Growth Polymerization" mechanism (RSGP mechanism) based on the recombination of reactive species and the subsequent reactivation of their product [17]. This model was later developed by "Competitive Ablation and Polymerization" (CAP), that is, concurrent etching and growth of the PPF [17–19].

Nevertheless, models were also developed to include an ionic contribution to the growth mechanism [20, 21]. Notably, the "Ion-Activated Growth Model" introduced by d'Agostino proposed chemical bond breaking of the exposed surface by bombarding ions (typically with kinetic energy varying from 10 to 30 eV), generating suitable reactive sites for adsorbed radicals of the plasma [22, 23]. Other studies suggested, for specific power conditions, an important contribution of the condensing ions to the film-forming species [24, 25]. Interestingly, Hegemann et al. demonstrated the effect of ionic bombardment (quantified by the concept of energy density) on the density and cross-linking degree of a PPF [26]. Finally, the effect of ultraviolet radiation, specifically the so-called short-wavelength "vacuum-ultraviolet" (VUV) emitted by plasma, has also been considered to affect the crosslinking degree of the material [27–30].

The role of the energy per precursor molecule, expressed by the Yasuda parameter W/FM (where W is the power dissipated in the plasma, F is the precursor flow, and M is the molecular mass of the precursor), was quickly identified as a determining factor for controlling the physicochemical properties of a PPF [31]. The growth rate typically increases linearly with the Yasuda parameter, a phenomenon explained by the higher activation of the chemical vapor, until a plateau is reached, corresponding to the monomer-deficient region—as most of the monomer was activated. In this regime, further increasing the power does not change the density of film-forming species. Furthermore, the chemical composition of PPF is also affected by the Yasuda parameter. Plasma polymerization conducted under low-energy conditions provides a low degree of precursor fragmentation and thus higher retention of the chemical group hosted by the precursor.

The choice of the precursor was also shown to drastically affect the growth rate and the chemical composition of the PPF [32]. Notably, unsaturated molecules lead to a relatively high deposition rate [4]. Finally, although rarely studied, it was demonstrated that the substrate temperature could also influence the growth rate of the plasma polymer through the adsorption/desorption equilibrium [33, 34]. In the case of atmospheric pressure plasma, an effect on the PPF structure and chemistry was also demonstrated [35]. It should also be mentioned that the study of plasma polymerization is impeded by the significant impact of the plasma chamber design on the process, making comparison of the results reported by different research groups difficult [36, 37]. More information about plasma polymerization and the history of the method can be found elsewhere [18, 38].

From these studies, it is clear that it is now possible to finely control the chemical composition of PPF, enabling the synthesis of coatings with tailor-made surface chemistry through the modulation of the energy injected in the discharge [32, 39].

Although the chemical composition has received considerable attention, the mechanical properties have been poorly investigated despite their importance in applications such as cellular growth [40]. It has been reported that Young's modulus of PPFs increases with the energy load, correlated to an increase in the cross-linking degree of the polymeric network [41]. Nevertheless, the control offered by the modulation of the power dissipated into the discharge is quite limited; Young's modulus of PPFs typically ranges from 0.5 to 10 GPa, limiting further development in the field [41–43]. Furthermore, the concept of glass transition, which is considered to be directly correlated to the viscoelastic properties of polymers, is most of the time overlooked in the context of PPF materials in the discussion of their mechanical properties.

Recently, we have demonstrated that the mechanical properties of PPF can be dramatically influenced using an almost unexplored approach, namely, regulation of the substrate temperature (T_S) during the growth of the PPF [33, 34]. Interestingly, the mechanical properties of propanethiol-based PPFs evolve from a high-viscosity liquid to a hard elastic solid (with Young's modulus of 9.94 ± 5.88 GPa) for a short range of T_S variation (i.e., from 10°C to 45°C), providing an avenue for the design of mechanically responsive PPFs of interest for flexible electronics [44, 45]. These data were correlated with the evolution of the glass transition temperature, highlighting that the mechanical response of the PPF is temperature-dependent [45, 46]. However, for similar experimental conditions, the physicochemical properties of propylamine-based PPFs were almost not affected by the thermal conditions of the substrate [47]. It can be concluded from these studies that an overall understanding about the exact role played by the surface temperature in the plasma polymerization mechanism and its impact on the viscoelastic and mechanical properties of PPFs has not clearly emerged, especially regarding the influence of the chemical precursor.

In this context, the main objective of this work is to further investigate the influence of the substrate temperature on the mechanical properties of PPFs and to correlate their evolution

16128869, 2024, 12, Downloaded from https://onlinelibrary.wiley.com/doi/10.1002/ppap.202400166 by Bibliothecaire En Chef Uni Catholique De Louvain (Ucl), Wiley Online Library on [27/01/2025]. See the Terms and Conditions (https://onlinelibrary.wiley.com/terms-and-conditions) on Wiley Online Library for rules of use; OA articles are governed by the applicable Creative Commons License

with the growth mechanism of the coatings. For this purpose, two precursors are considered, differing only by their unsaturation degree: allyl alcohol (CH_2=CH–CH_2–OH) and propanol (CH_3–CH_2–CH_2–OH). A systematic investigation of the mechanical and viscoelastic properties (by using cutting-edge scanning probe microscopy and spectroscopy), the glass transition temperature (time of flight-secondary ions mass spectrometry [ToF-SIMS]), the chemical composition (X-ray photoelectron spectroscopy [XPS]), the cross-linking degree (ToF-SIMS), and the deposition kinetics is undertaken and correlated to the plasma chemistry.

2 | Experimental Section

2.1 | Reagents

2-propen-1-ol (99%, Sigma-Aldrich) and propan-1-ol (99%, Sigma-Aldrich), which will, respectively, be referred to as allyl alcohol and propanol in this work, were used as received for the plasma polymerization process. The fabricant value for the boiling point is 96–98°C for allyl alcohol and 97°C for propanol, and the vapor pressure is 23.8 mmHg at 25°C for allyl alcohol and 14.8 mmHg at 20°C for propanol. PPFs were deposited on $1 \times 1\ cm^2$ silicon wafers. Before their introduction into the plasma chamber, the substrates were cleaned with 1-isopropanol three times and dried under a nitrogen flow.

2.2 | Plasma Polymerization Method

PPF growth was carried out in a metallic deposition chamber (65 cm in length and 35 cm in diameter) with a residual pressure of less than 2.10^{-6} Torr (i.e., 2.7×10^{-4} Pa). The vacuum was ensured by the use of a combination of turbomolecular and primary pumps. A more detailed description of the plasma chamber can be found elsewhere [5]. The reactor consists of an internal one-turn inductive copper coil (10 cm in diameter) cooled with water connected to an Advanced Energy Radio-frequency (13.56 MHz) power supply with a matching network. For all the experiments, an inductively coupled plasma (ICP) in capacitive mode was generated with a dissipated power of 40 W. The liquid precursor (allyl alcohol or propanol) was stored in a heated tank (200 mL) at 60°C to ensure sufficient vapor pressure. A mass flow meter supplied by Omicron allowed fine control of the precursor flow rate, fixed at 10 sccm for this study. No other gas was added in the chamber during the experiments in order to generate the plasma with pure vapor of the selected precursor. The distance separating the substrate from the coil was fixed at 10 cm. A throttle valve was connected to a capacitive gauge to ensure a constant working pressure of 40 mTorr during the process. The substrate temperature, that is, the temperature of the substrate holder on which $1 \times 1\ cm^2$ silicon wafers are mounted, was controlled by a combination of liquid nitrogen flow in the manipulator (for cooling) and electrical resistances in the substrate holder (heating) coupled with a thermocouple, also inside the substrate holder. This system allowed to control the temperature with a precision of ±1°C. Five temperatures have been investigated in this work, namely, −10°C, 0°C, 10°C, 23°C, and 45°C. Before each deposition, the substrate temperature was stabilized for 30 min to ensure thermal equilibrium between the silicon substrate and the heating/cooling system. For the sake of simplicity, the following notation will be used to reference the various PPFs used in this work: PPFs synthesized with allyl alcohol at a substrate temperature "X"°C will be denoted as allyl-$PPF_{X°C}$, whereas those obtained with propanol will be denoted as prop-$PPF_{X°C}$.

For each experiment, the PPF deposition was calibrated to obtain a thickness of 220 nm, with the exception of thickness measurements, which were performed on samples with thicknesses ranging from 100 to 300 nm.

2.3 | Thickness Measurements

The deposited film thicknesses for each precursor were determined by scratching the coating surface with a scalpel blade and measuring the depth of the step produced by AFM measurement. The apparatus consists of a Bruker Multimode 8 microscope (Tapping Mode) associated with a Nanoscope III controller. The growth rate was obtained from the measured thickness versus the deposition time. Thickness measurements were performed on samples with thicknesses ranging from 100 to 300 nm.

2.4 | XPS Measurement

The chemical composition of PPFs was investigated by XPS. The measurements were carried out using a PHI 5000 VersaProbe apparatus under a pressure of 5×10^{-9} Torr (ca. 6.5×10^{-7} Pa). The photon source was a monochromatized Al Kα line (1486.6 eV). The emitted photoelectrons were collected at an angle of 45° with respect to the surface. The samples were analyzed ex situ directly after their synthesis to ensure minimal air contamination. Consequently, PPFs were exposed for 10 min to ambient air during the transfer from the plasma chamber to the XPS apparatus. Each sample was analyzed at three different areas to ensure its homogeneity. High-resolution C1s spectra were curve-fitted using Multi-Pak software and considering a Gaussian–Lorentzian function (70% Gaussian) with a full width at half-maximum of 1.0–1.5 eV.

2.5 | Cross-Linking Degree Evaluation

The cross-linking degrees were studied using ToF-SIMS measurements. Samples were probed immediately after their synthesis to avoid air contamination. Static ToF-SIMS data were acquired in positive mode. Prop-PPF were investigated at room temperature with a ToF-SIMS IV instrument supplied by ION TOF GmbH using a pulsed 10 keV Ar^+ ion beam (0.75 pA) rastering a scan area of $300 \times 300\ \mu m^2$ eight times for each sample. Allyl-PPF were probed at a temperature of −30°C, significantly below their glass transition temperature, using a ToF-SIMS V instrument supplied by ION TOF GmbH. A 30 keV Bi_5^+ ion beam (0.04 pA) rastered a scan area of $500 \times 500\ \mu m^2$ three times for each sample. The allyl-PPF temperature was controlled during the analysis with a special holder called

16128869, 2024, 12, Downloaded from https://onlinelibrary.wiley.com/doi/10.1002/ppap.202400166 by Bibliothecaire En Chef Uni Catholique De Louvain (Ucl), Wiley Online Library on [27/01/2025]. See the Terms and Conditions (https://onlinelibrary.wiley.com/terms-and-conditions) on Wiley Online Library for rules of use; OA articles are governed by the applicable Creative Commons License

"Holder G," also provided by ION TOF GmbH, allowing to maintain the sample at any temperature between −150°C and 600°C with an accuracy of ±1°C. The analyte temperature was stabilized 20 min before analysis to ensure its thermal equilibrium. The ToF-SIMS mass spectra were normalized to the total ion count number and analyzed using a statistical method called Principal Component Analysis (PCA) using SIMCA-13 software supplied by Umetrics (Sweden).

PCA is a multivariate analysis technique aiming at summarizing the variance patterns within a data set. The variance in the data describes the differences between the samples. For ToF-SIMS data, these differences arise from changes in the relative intensity of the peaks between the sample spectra. Using PCA, a new set of axes called principal components (PCi) is created, defining the directions of the major variations within the data set. PC1 describes the line that best approximates the data. Usually, one PCi is not enough to model the variance of a data set. A second PCi (PC2), orthogonal to PC1, is then calculated to improve the data approximation and so on. The results are then interpreted using specific concepts, namely, the "scores" and the "loadings." The scores describe the relationship between the samples synthesized at each T_S, whereas the loadings reveal the ionized fragments responsible for the differences between the samples. More information about this multivariate analysis method and its uses in plasma investigation can be found elsewhere [43, 48, 49].

2.6 | Surface Transition Temperature Evaluation

Glass transition temperature of the samples were estimated using a recently developed method based on ToF-SIMS measurements [50, 51]. Static ToF-SIMS data were acquired using a ToF-SIMS V instrument supplied by ION TOF GmbH. An Ar gas cluster ion beam (Ar-GCIB) with a cluster distribution centered on Ar_{3000}^+ was raster-scanned over an area of $500 \times 500\,\mu m^2$ (128×128 data points). Ar cluster ions were accelerated toward the surface with an energy of 10 keV. A low-energy (5 eV) electron flood gun was used to avoid charging effects of the probed sample. Before each analysis, the analyte temperature was stabilized 20 min before analysis to ensure the thermal equilibrium of the PPF and potential surface contamination was removed by pre-sputtering of 2×10^{13} Ar_{3000}^+/cm^2 in DC mode over an area of $1000 \times 1000\,\mu m^2$. The thickness of the probed PPF was fixed at 220 nm to avoid any substrate effect on the measurement. Analysis of the ToF-SIMS data, specifically the Ar_2^+ and Ar_3^+ peak intensities, was performed to determine the surface transition temperature (T_T), strongly correlated to the bulk glass transition temperature (T_g).

2.7 | Mechanical and Viscoelastic Characterization

The mechanical and viscoelastic properties of PPFs were probed by Peak-Force Tapping Quantitative Nanomechanical Mapping (PF-QNM) [52, 53]. Measurements were performed using a Bruker AFM ICON Dimension equipped with a Nanoscope 5 Controller. PF-QNM data were collected using pre-calibrated AFM tips (RTESPA300-30) supplied by Bruker with a calibrated spring constant k of ±50 N/m and tip radius of ±25 nm. Before the analysis, the deflection sensitivity was calibrated on sapphire and found to be 45.54 ± 7.62 nm/V. The rigidity modulus values were extracted by fitting part of the retract curve with the Johnson–Kendall–Roberts (JKR) model. JKR has been proven to be effective previously in the analysis of deformable materials, notably PPF [45]. More information about the JKR theory and its describing equations can be found elsewhere [54]. Three measurements were performed for each sample using different areas. The thickness of the probed PPF was fixed at 220 nm to avoid any impact of the substrate on the AFM measurements.

PPFs' fluid-like behavior was evaluated using a "scratch" method recently developed for the analysis of thin films [45]. Deformation was generated by sweeping the film surface with the AFM tip in Contact Mode following a unidirectional line of 5 μm. For a liquid coating, the resulting scratch should recover over time. To study the relaxation dynamics, the perturbation topography was regularly imaged using AFM in Tapping Mode at an angle of 90° compared to the Contact Mode angle. For both the scratching and the imaging of the surface, a deflection setpoint of 25 nN was used. The scratch experiments were performed using a Bruker AFM ICON Dimension equipped with a Nanoscope 5 Controller. Pre-calibrated AFM tips SCM-PIT-V2 were supplied by Bruker ($k = \pm 3$ N/m).

2.8 | Mass Spectrometry

The plasma composition was probed using a quadrupole HAL EQP 1000 mass spectrometer provided by Hidden Analytical. A 100 μm extraction orifice connected the spectrometer to the plasma chamber. The neutral plasma species were investigated in residual gas analysis (RGA) mode. Radicals and molecules were ionized by electron impact (EI) with a low kinetic energy of 20 eV to limit their fragmentation in the spectrometer. For the sake of clarity, the mass spectra are presented from $m/z = 1$ to 65, as no significant peak is observed for $m/z > 60$.

3 | Results and Discussion

3.1 | Results

The mechanical properties of prop-PPF and allyl-PPF have been probed using the AFM Peak-Force QNM method [55]. Typical force–distance curves of these samples are presented in Figures 1a,b. These curves represent the forces exerted on the AFM tip during its approach (straight lines) and its removal (doted lines) from the probed surface. At the beginning of the measurement (distance = 0 nm), the force is zero or very low, as the AFM tip is far from the surface and not interacting with it. At a given distance during the approach, attractive forces between the surface and the tip will pull the cantilever toward the surface, which is represented by a negative force. As the cantilever keeps advancing, the force registered increases, becoming positive when the tip starts applying pressure on the sample. The approach is stopped when the peak force is reached, here at 30 nN. The tip then withdraws: the force

16128869, 2024, 12, Downloaded from https://onlinelibrary.wiley.com/doi/10.1002/ppap.202400166 by Bibliothecaire En Chef Uni Catholique De Louvain (Ucl), Wiley Online Library on [27/01/2025]. See the Terms and Conditions (https://onlinelibrary.wiley.com/terms-and-conditions) on Wiley Online Library for rules of use; OA articles are governed by the applicable Creative Commons License

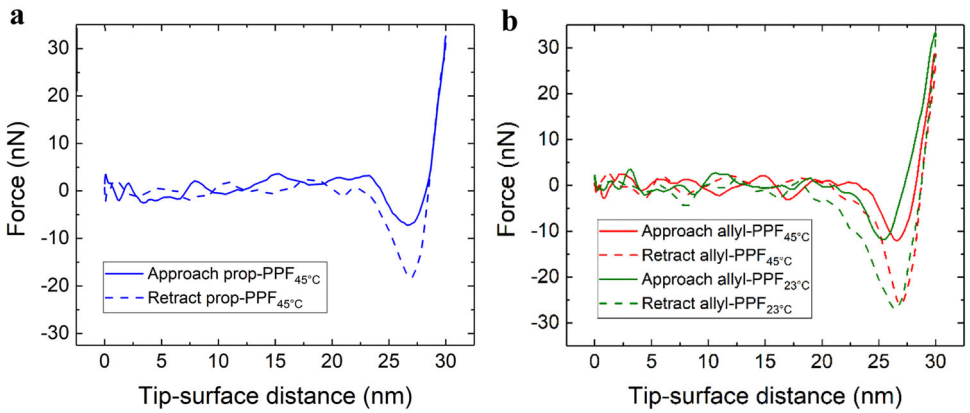

FIGURE 1 | Force–displacement curves for prop-PPF (a) synthesized at 45°C and for allyl-PPF (b) synthesized at 23°C (green) and 45°C (red). The approach curves are represented by a straight line and the retract curves are represented by a dashed line.

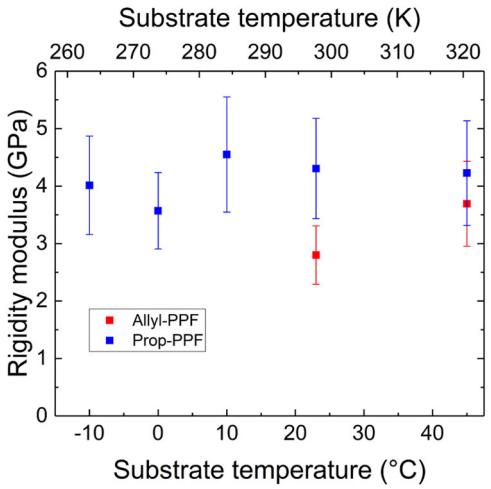

FIGURE 2 | Evolution of the rigidity modulus for allyl alcohol (red) and propanol (blue) PPF as a function of the substrate temperature.

decreases as the cantilever moves away from the surface [56, 57].

The curves were fitted using the JKR model, as already applied to probe PPF [45, 47, 54]. This analysis allows the determination of the rigidity modulus (E_M) characterizing the elastic behavior of the probed thin film. As the root-mean-square (RMS) roughness is below 1.2 nm for all PPFs, the rigidity modulus measurements are assumed to be independent of the PPF topography. Figure 2 reports the evolution of E_M for both PPF families as a function of T_S.

The rigidity modulus of prop-PPF remains stable at around 4 GPa regardless of T_S, considering the confidence intervals. This rigidity modulus value corresponds to the ones typically reported in the literature for different precursors in similar deposition conditions [43, 45, 47].

For Allyl-PPF, E_M is found to increase from 2.8 ± 0.8 to 3.7 ± 0.7 GPa for T_S ranging from 23°C to 45°C. Analysis of the recorded force–distance curves, presented in Figure 1b, shows a more significant separation between the approach and the retract curves at lower substrate temperatures,

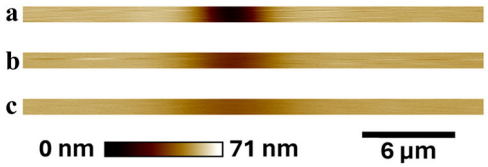

FIGURE 3 | Topographic AFM images (256×10 data points) of allyl-$PPF_{0°C}$ after a "scratch" deformation of the thin-film surface. The recovery time of the deformation is 100 s (a), 700 s (b), and 2500 s (c).

suggesting higher energy dissipation and hence viscous component.

For $T_s \leq 10$°C, the shape of the recorded approach–retract curve makes any mathematical treatment for extracting the mechanical properties unfeasible, as already observed for propanethiol-based PPFs considering similar experimental conditions [45]. In a previous study investigating the relaxation dynamics of a scratch induced on the propanethiol-based PPF surface with the AFM tip, it was concluded that the material behaves like a high-viscosity liquid at low T_S [45]. In this context, a similar approach is applied here for allyl-PPF synthesized for $T_S \leq 10$°C. The AFM Contact Mode is used to sweep the surface with a force of 25 nN along a distance of 10 µm, consequently scratching the PPF. The temporal evolution of the perturbation topography is then recorded with the AFM in Tapping Mode, as illustrated in Figure 3 for allyl-$PPF_{0°C}$.

AFM line profiles of a scratched allyl-$PPF_{0°C}$ after different recovery times are shown in Figure 4a. It can be seen that the scratch refills through matter movement as a function of time. Indeed, the deformation depth is initially about 60 nm but quickly decreases, whereas the scratch spreads through the PPF surface over time as also shown in Figure 4b depicting the time evolution of the scratches full width at half maximum (FWMH) for allyl-$PPF_{10°C}$, allyl-$PPF_{0°C}$, and allyl-$PPF_{-10°C}$.

It has been reported that, considering a liquid thin film, the FWHM is supposed to follow a power law as a function of t [45]:

$$L \sim \left(\frac{\gamma}{\eta} h_o^3\right)^{1/4} t^{1/4}, \quad (1)$$

16128869, 2024, 12, Downloaded from https://onlinelibrary.wiley.com/doi/10.1002/ppap.202400166 by Bibliothecaire En Chef Uni Catholique De Louvain (Ucl), Wiley Online Library on [27/01/2025]. See the Terms and Conditions (https://onlinelibrary.wiley.com/terms-and-conditions) on Wiley Online Library for rules of use; OA articles are governed by the applicable Creative Commons License

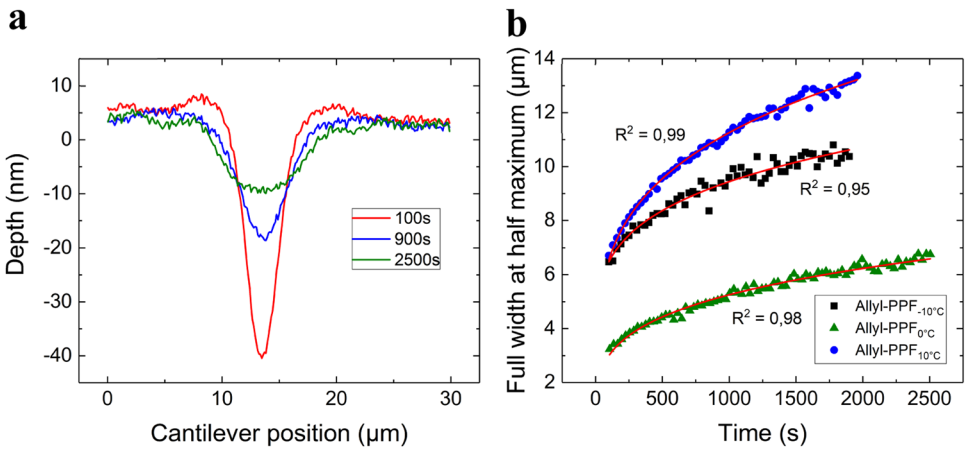

FIGURE 4 | (a) AFM line profiles of a scratched allyl-$PPF_{0°C}$ for various recovery times. (b) Evolution of the deformation full width at half maximum over time for allyl-$PPF_{-10°C}$ (dark square), allyl-$PPF_{0°C}$ (green triangle), and allyl-$PPF_{10°C}$ (blue circle).

where L is the FWHM of the perturbation, γ is the surface tension, η is the viscosity, h_o is the thickness of the film, and t is the time.

As shown in Figure 4b (red lines), this power law adequately fits the experimental data unambiguously, indicating the liquid nature of these materials. The viscosity η of these liquid PPFs can be evaluated from the fitting procedure according to Equation (1) considering a surface tension value (γ) of 10^{-2} N/m and a PPF thickness (h_o) of 2.10^{-7} m. The obtained PPF viscosity values are estimated to be around 10 Pa.s for $T_S = -10°C$ and 10°C and around 10^2 Pa s for $T_S = 0°C$. Considering the increase in E_M with T_S from the PF-QNM measurements of allyl-PPF, the viscosity of allyl-PPF prepared at $T_S \leq 10°C$ probably slightly evolves with T_S but this evolution cannot be characterized using the present technique, likely due to the sensitivity limit of the measurement.

At this stage, the investigation of the mechanical properties reveals drastic variations regarding the source molecule. Although allyl-PPF shows a transition from a high-viscosity liquid to a hard elastic material for T_S ranging from −10°C to 45°C, the thermal conditions of the substrate have no influence on prop-PPF showing a solid behavior with a rigidity modulus of about 4 GPa irrespective of the value of T_S.

Considering conventional polymerization, the mechanical properties of polymers synthesized from the same monomer can vary, evolving from a liquid to an elastic solid, as a function of their glass transition temperature (T_g) [58, 59]. Therefore, the evaluation of T_g can provide information about the evolution of the mechanical properties of the materials regarding the source molecule and T_S.

On this basis, the glass transition temperature of both PPF families has been investigated using a ToF-SIMS method recently developed by Poleunis et. al. [45, 50] Briefly, the method consists of measuring the rate of backscattered Ar_n^+ ions from Ar_{3000}^+ clusters during ToF-SIMS measurements carried out on samples at different analysis temperatures.

They found that the $Ar_2^+/(Ar_2^+ + Ar_3^+)$ ratio dramatically evolves at a temperature close to their T_g, as evaluated by conventional differential scanning calorimetry. This ratio follows a sigmoidal trend as a function of the analysis temperature. The temperature corresponding to the inflexion point is called the surface transition temperature (T_T) of the material and is directly correlated to the glass transition temperature [50]. This method has been successfully applied to probe the surface transition temperature of propanethiol and propylamine PPFs [47].

Figure 5a and 5b depict the recorded curves for, respectively, prop-PPF and allyl-PPF, both of which show a sigmoid shape in line with the literature. For both precursors, the T_T increases with the substrate temperature (Figure 5c). Also, irrespective of the substrate temperature, the T_T of prop-PPF was systematically higher (i.e., from 37.5 ± 2.5 to 92.5 ± 2.5°C) than the room temperature, meaning that the AFM analysis performed on those films was performed at a temperature below their T_T. This explains the elastic solid behavior deduced from the AFM measurements irrespective of the value of T_S.

Meanwhile, allyl-PPF presents a T_T ranging from 17.5 ± 5°C to 75 ± 10°C, in perfect agreement with the previously reported AFM measurements. Indeed, the PPF viscosity for $T_s \leq 10$°C did not vary significantly with T_s, and the T_T are rather close to each other and below T_{room}, explaining why the material behaves like a liquid. Allyl-$PPF_{23°C}$ ($T_T \approx T_{room}$) showed viscoelastic behavior, whereas allyl-$PPF_{45°C}$ behaves like an elastic solid film, as T_T (i.e., $75 \pm 10°C$) > T_{room}. Interestingly, a previous study has reported T_g values measured by DRS (Dielectric Relaxation Spectroscopy) for allyl alcohol plasma polymer to be in the range of 40–150°C, in line with our measurements [7].

In conventional polymers, it is well known that the cross-linking degree χ and the chemical composition can drastically influence the T_g of the material and hence its mechanical properties [58, 60]. In order to better understand the evolution of T_T, the cross-linking degree and the chemical composition of PPFs with T_S were investigated by means of ToF-SIMS and XPS analysis, respectively.

16128869, 2024, 12, Downloaded from https://onlinelibrary.wiley.com/doi/10.1002/ppap.202400166 by Bibliothecaire En Chef Uni Catholique De Louvain (Ucl), Wiley Online Library on [27/01/2025]. See the Terms and Conditions (https://onlinelibrary.wiley.com/terms-and-conditions) on Wiley Online Library for rules of use; OA articles are governed by the applicable Creative Commons License

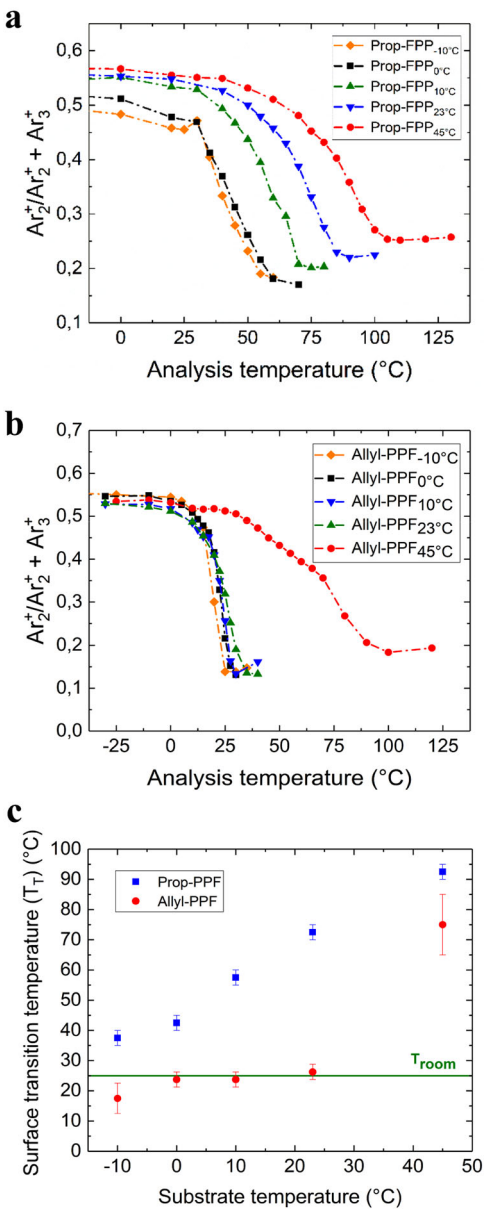

FIGURE 5 | $Ar_2^+/(Ar_2^+ + Ar_3^+)$ ratio of backscattered ions collected during the sputtering of Ar_{3000}^+ ions on the surface of prop-PPF (a) and allyl-PPF (b) at various temperatures. (c) The resulting curves are used to determine the surface transition temperature (T_T) for prop-PPF (blue square) and for allyl-PPF (red circle). The green line shows the room temperature used for analysis of mechanical and viscoelastic properties.

Supporting Information S1: Figure S1a and S1b present typical XPS survey spectra for prop-PPF and allyl-PPF, respectively. For both precursors, XPS analysis reveals only the presence of carbon and oxygen. As shown in Figure 6, the atomic oxygen concentration remains constant for a given precursor (i.e., ~19% for allyl-PPF and ~7% for prop-PPF compared to the original 25% of the precursors) considering the confidence intervals. Allyl-PPF shows a higher oxygen content than prop-PPF, whereas both have a lower oxygen proportion than their corresponding precursor, as is usually found in the literature [61]. The higher oxygen content of allyl-PPF is usually explained by conventional polymerization of the allyl alcohol precursor thanks to its double bond [7, 61]. However, allylic

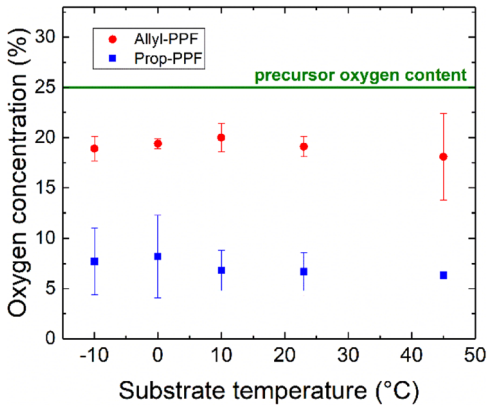

FIGURE 6 | Evolution of the oxygen concentration of allyl-PPF (red) and prop-PPF (blue) with the substrate temperature.

monomers are susceptible to degradative chain transfer, which consists of the migration of an H in the α position, leading to the formation of a resonance-stabilized radical [62]. This species is unlikely to propagate the polymer chain and will eventually react with another radical, ending the polymerization process. An example of degradative chain transfer for allyl alcohol is illustrated in Supporting Information S1: Figure S2. It should be mentioned that the oxygen concentrations might be slightly overestimated due to post-synthesis oxidation reactions. Indeed, it is well known that radicals trapped in the PPF react with dioxygen and water, from which exposition in ambient air is unavoidable while transferring a sample from the plasma chamber to the XPS [63].

However, the oxygen content provides no detail about the chemical environment of the heteroelement as a function of T_S. Therefore, the envelope of the C1s peaks from XPS spectra has been fitted. For both precursors, the deconvolution of the envelope reveals the presence of three components associated with different carbon bonding: C–C/C–H at 284.9 eV, C–O–H/C–O–C (alcohol or ether functions) at 286.3 eV and C═O (carbonyl and aldehyde functions) at 287.7 eV. The choice and the labeling of these different components are based on the reported detailed chemical investigations of O-based PPFs, the wide variety of functional groups being explained by the numerous recombinations and rearrangements of precursor fragments forming the coating [7, 64–66]. A typical fitting of the high-resolution C1s peak for prop-PPF and allyl-PPF is presented in Figure S3a and S3b, respectively.

Figure 7a,b shows the relative concentrations of different functional groups obtained by deconvolution of C1s peaks. As is usually reported in the literature, new functionalities that are not present in the precursor structure are created following the plasma polymerization process (e.g., ketones, ethers) [7]. Comparing both precursors, concentrations of oxygen-containing functionalities are twice as important in allyl alcohol spectra (25% for C–O and 5.2% for C═O) compared to propanol XPS spectra (11% for C–O and 2.6% for C═O), in agreement with the higher incorporation of oxygen into allyl alcohol-based plasma polymers. It should be highlighted that the higher concentration of oxygen likely contributes to an intrinsic lower cross-linking degree for allyl alcohol, the valence state of oxygen being only two compared to four for a carbon atom.

16128869, 2024, 12, Downloaded from https://onlinelibrary.wiley.com/doi/10.1002/ppap.202400166 by Bibliothecaire En Chef Uni Catholique De Louvain (Ucl), Wiley Online Library on [27/01/2025]. See the Terms and Conditions (https://onlinelibrary.wiley.com/terms-and-conditions) on Wiley Online Library for rules of use; OA articles are governed by the applicable Creative Commons License

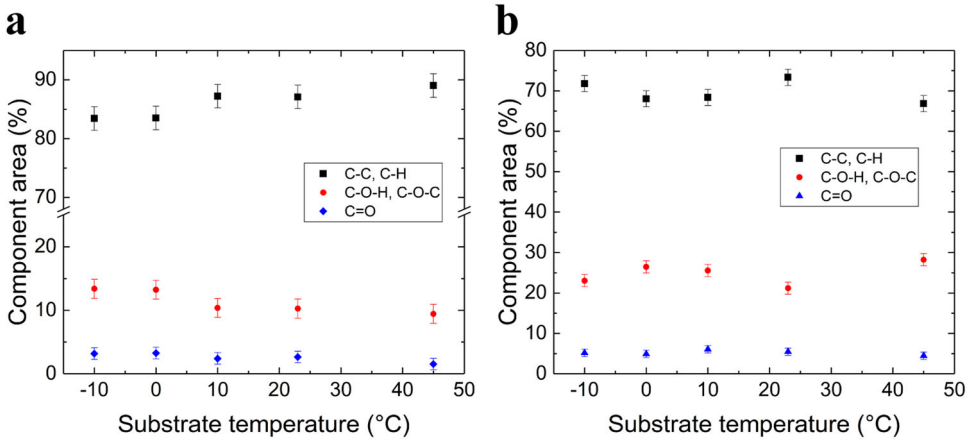

FIGURE 7 | Evolution of the components' relative area resulting from the fitting of the high-resolution C1s peak for prop-PPF (a) and allyl-PPF (b). For both precursors, three components are distinguished and associated with C–C/C–H (black), C–O–H/C–O–C (red), and C═O (blue).

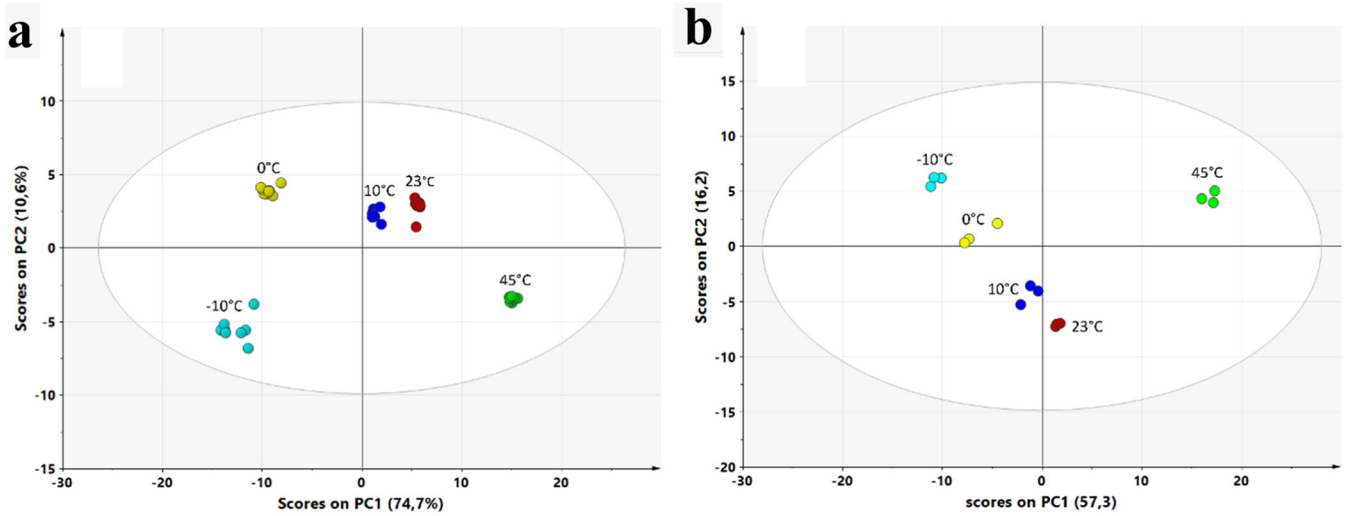

FIGURE 8 | Score plots depicting sample discrimination based on the PCA processing of the ToF-SIMS data for prop-PPF (a) and allyl-PPF (b).

Furthermore, the chemical composition is likely to influence the interchain interactions, in turn, affecting their mobility and thus the T_g, which might explain the differences in terms of mechanical properties for both plasma polymer families.

However, for a given precursor, the relative concentration of the different components remains rather stable with T_S in contrast with the evolution of T_T. Therefore, the evolution of T_T with T_S cannot be explained by the chemical composition of the PPF. In this context, the evolution of χ, known as another influential factor on T_g of polymers, has been investigated by ToF-SIMS measurements.

An example of ToF-SIMS spectra corresponding to allyl-PPF$_{10°C}$ is presented in Supporting Information S1: Figure S4. As is usually found for the analysis of PPFs, numerous peaks with various intensities can be observed, making establishment of specific trends regarding the impact of T_S on the PPF physicochemical properties extremely challenging. To overcome this issue and to extract the most important chemical and structural information about the analyzed materials, the PCA method has been used [48]. This method has already been used to characterize the evolution of χ in PPFs [43, 49, 66–68].

Figure 8a and 8b show the resulting "score" plot from the PCA treatment of the ToF-SIMS data corresponding to the analysis of prop-PPF and allyl-PPF, respectively. In this plot, each individual point in the figure represents a whole ToF-SIMS spectrum. The larger the distance between the points, the larger the difference between the corresponding ToF-SIMS spectra, revealing variations in terms of the surface structure and/or chemistry. The ellipse drawn on the scores plot represents a 95% confidence interval. It can be observed that for each PPF family, most of the variance is captured by PC1 (i.e., 74.7% and 57.3% for prop-PPF and allyl-PPF, respectively). Therefore, only PC1 has been considered to analyze the results.

It can be observed that, within a PPF family, the spectra are divided into rather small clusters as a function of T_S, although their distinction can eventually be difficult (e.g., allyl-PPF$_{10°C}$ and allyl-PPF$_{23°C}$). Therefore, the mean value of scores has been evaluated as a function of T_S to rationalize their discrimination along PC1. It can be observed from Table 1, for each PPF family, that the scores are well discriminated as a function of T_S along PC1 considering the confidence interval. This reveals a modification of χ and/or the chemical composition of the PPF with T_S.

16128869, 2024, 12, Downloaded from https://onlinelibrary.wiley.com/doi/10.1002/ppap.202400166 by Bibliothecaire En Chef Uni Catholique De Louvain (Ucl), Wiley Online Library on [27/01/2025]. See the Terms and Conditions (https://onlinelibrary.wiley.com/terms-and-conditions) on Wiley Online Library for rules of use; OA articles are governed by the applicable Creative Commons License

TABLE 1 | Mean score plot (PC1) as a function of T_S revealed by the PCA analysis of the positive ToF-SIMS data of prop-PPF and allyl-PPF (Figure 8a and 8b, respectively).

	Substrate temperature (°C)				
	−10	**0**	**10**	**23**	**45**
Prop-PPF	-12.65 ± 1.31	-9.35 ± 0.66	1.33 ± 0.36	5.60 ± 0.21	15.07 ± 0.29
Allyl-PPF	-10.67 ± 0.52	-6.51 ± 0.92	-1.22 ± 0.88	1.57 ± 0.22	16.83 ± 0.73

TABLE 2 | Average fragments and their corresponding C/H ratio of the most influential loadings (statistical weight > 80%) resulting from the PCA of the prop-PPF spectra. The substrate temperature associated with the positive and negative scores is also provided.

Prop-PPF	**Negative loadings**	**Positive loadings**
Average fragment	$C_{7.03}H_{11.4}$	$C_{4.66}H_{5.47}$
C/H ratio	0.619	0.851
Substrate temperature	−10°C; 0°C	10°C; 23°C; 45°C

TABLE 3 | Average fragments and their corresponding C/H ratio of the most influential loadings (statistical weight > 80%) resulting from the PCA of the allyl-PPF spectra. The substrate temperature associated with the positive and negative scores is also provided.

Allyl-PPF	**Negative loadings**	**Positive loadings**
Average fragment	$C_{7.02}H_{10.27}$	$C_{4.17}H_{5.10}$
C/H ratio	0.684	0.818
Substrate temperature	−10°C; 0°C; 10°C	23°C; 45°C

Tables S1a,b and S2a,b summarize the most statistically important peaks called "loadings" for each PPF family (i.e., peaks with a statistical weight > 80%) in the PC1 model, responsible for sample discrimination in the score plot. A positive or negative loading coefficient (yielding the statistical weight) is associated with each m/z signal. The higher the absolute value of the loading coefficient, the higher the relative intensity variation of the corresponding peak from one sample to another.

To obtain information about χ, the average chemical composition of the fragments has been calculated for each loading category (negative and positive) considering each PPF family [49]. In the first approach, all oxygen atoms present in these ionized fragments have been replaced by CH_2, which are of identical valence state. The corresponding data are summarized in Tables 2 and 3 for prop-PPF and allyl-PPF, respectively.

From the average fragment, particular attention is paid to the carbon to hydrogen ratio (C/H) correlated with χ of the PPF [43]. It is noteworthy that this ratio is also influenced by the potential presence of double/triple bonds and cycle in the PPF. However, as already demonstrated for several PPF families from (FT)IR analyses, the presence of unsaturation can be excluded [4, 69]. Thus, it can be reasonably assumed that, here, the C/H ratio reflects the PPF cross-linking degree. It can be observed from Tables 2 and 3 that the C/H ratio increases with T_S (i.e., from 0.619 to 0.851 for prop-PPF and from 0.684 to 0.818 for allyl-PPF), implying an increase in χ of the PPF as a function of T_S. The latter correlates the evolution of T_T for both precursors. Indeed, the increase in χ reduces the mobility of the molecular segments, resulting in an increase in T_T.

At this stage, it can be concluded that the evolution of T_T observed previously can mainly be explained by an increase in χ when T_S increases for each PPF family. However, the origin of this evolution of χ with T_S has not yet been elucidated. Furthermore, the reason for the variation of T_T with T_S (from below to above T_{room} or only above) strongly differing between both precursors remains unclear. One could postulate that χ of prop-PPF (elastic regardless of T_S) is higher than that of allyl-PPF (liquid or viscoelastic as a function of T_S). Nevertheless, this hypothesis cannot be validated on the basis of ToF-SIMS measurements as it is difficult to compare χ for two different PPF families.

Therefore, to further investigate the influence of the chemical nature of the precursor on the PPF physicochemical properties, plasma chemistries are examined by mass spectrometry measurements in RGA mode aiming at identifying the neutral species produced in the discharge. Indeed, as already mentioned, for the conditions used in this work, the neutrals are considered to be the main contributing species to the PPF formation. The spectra collected from propanol and allyl alcohol discharges are depicted in Figure 9a and 9d, respectively.

Particular attention is paid to the peak corresponding to the precursor (i.e., $m/z = 60$ and 58 for prop-PPF and allyl-PPF, respectively), as previous studies correlated the heteroelement concentration in the PPF to the amount of non-fragmented precursor [6]. Then, the fragmentation degree (α) of the monomer is calculated according to

$$\alpha = 1 - \frac{I_{prec.}\ \text{(Plasma ON)}}{I_{prec.}\ \text{(Plasma OFF)}}, \quad (2)$$

where $I_{prec.}$ (Plasma ON) and $I_{prec.}$ (Plasma OFF) represent the experimental peak intensity for the precursor when the plasma is switched ON and OFF, respectively.

The measured mass spectra when the plasma is switched OFF for propanol and allyl alcohol are represented in Figure 9b and 9e, respectively.

The calculated value of α for each precursor is shown in Figure 10. It can be observed that the fragmentation degree of allyl alcohol (0.76 ± 0.05) is higher than that of propanol

16128869, 2024, 12, Downloaded from https://onlinelibrary.wiley.com/doi/10.1002/ppap.202400166 by Bibliothecaire En Chef Uni Catholique De Louvain (Ucl), Wiley Online Library on [27/01/2025]. See the Terms and Conditions (https://onlinelibrary.wiley.com/terms-and-conditions) on Wiley Online Library for rules of use; OA articles are governed by the applicable Creative Commons License

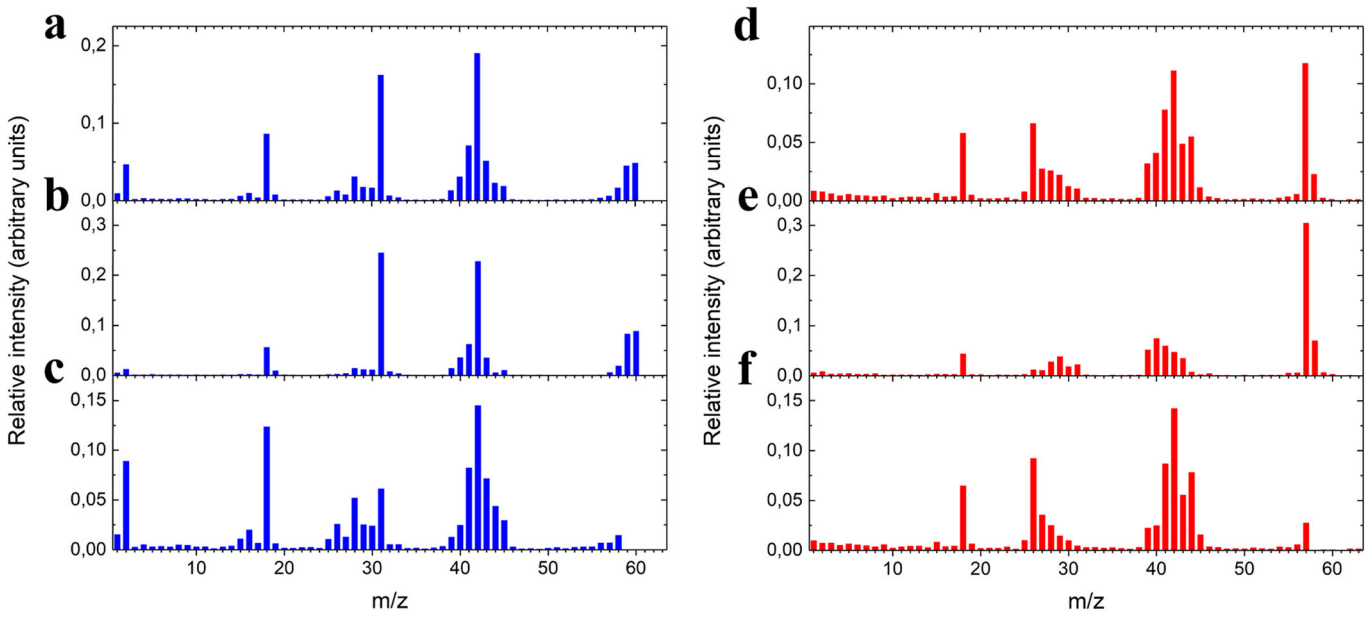

FIGURE 9 | Mass spectra of propanol discharge (Plasma ON) (a), propanol vapor (Plasma OFF) (b), and propanol plasma treated according to Equation (3) (c) are shown in blue. Mass spectra of allyl alcohol discharge (Plasma ON) (d), allyl alcohol vapor (Plasma OFF) (e), and allyl alcohol plasma treated according to Equation (3) (f) are presented in red.

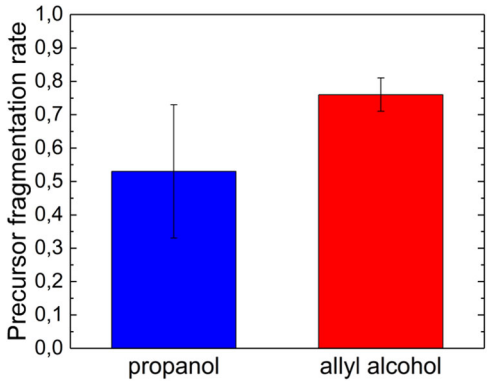

FIGURE 10 | Precursor fragmentation rate of propanol and allyl alcohol in their corresponding discharge.

(0.53 ± 0.20). These data cannot be correlated to the chemical composition of the PPF evaluated by XPS, a higher fragmentation rate being usually associated with lower functional group retention [6]. It should be noted that the fragmentation rates of the precursor governing the concentration of film-forming species also probably influence the deposition rate of each PPF, as will be discussed later.

For a more in-depth analysis of the plasma chemistry, the mass spectra have been further analyzed. It should be emphasized that neutrals collected from the plasma must be ionized to enable their discrimination in the mass analyzer according to the m/z ratio. The newly formed ions may be in an excited state and their excess energy can lead to the fragmentation of the molecular ion, hence resulting in the appearance of additional peaks in the mass spectrum. This explains why a mass spectrum with various peaks is collected even when the plasma is switched OFF. Therefore, except for the precursor, the detection of a signal in the mass spectrum does not necessarily mean that the corresponding species is present in the plasma. On this basis, in order to take into account the fragmentation of the precursor in the spectrometer itself, each signal recorded in the plasma was treated with the following equation [70]:

$$I_c(m) = I_g(\text{Plasma ON}) - I_g(\text{Plasma OFF}) \cdot \frac{I_{\text{prec.}}(\text{Plasma ON})}{I_{\text{prec.}}(\text{Plasma OFF})}, \quad (3)$$

where I_c (m) is the corrected peak intensity for $m/z = g$; I_g (Plasma ON) and I_g (Plasma OFF) represent the experimental peak intensity for $m/z = g$ when the plasma is switched ON and OFF, respectively. The corrected mass spectra for propanol and allyl alcohol are presented in Figure 8c and 8f, respectively. In this case, the appearance of a peak means that the corresponding species is produced in the plasma.

The main fragments identified in the mass spectra (in Figure 10a–f) are listed in Table 4. For the sake of simplicity, the ion corresponding to the precursor composition missing one hydrogen or several hydrogens is represented by $(M\text{-}xH)^+$, where x is the number of hydrogens missing from the original structure. For both precursors, numerous signals are identified, revealing the considerable diversity of species formed in the plasma (see Table 4 for the labeling). Regardless of the precursor, carbon-based species containing or not oxygen (C_yH_x and $C_yH_xO_z$) and hydrogenated species mixed with oxygen (H_xO) are observed. Several similitudes between the two precursors can be highlighted, such as the presence of peak clusters centered at $m/z = 28$ and 42, for instance, although the peak intensities may vary. This is not surprising considering that allyl alcohol and propanol have similar hydrocarbon backbones and contain the same heteroelement, thus leading to fragments with similar m/z. However, several differences are also observed between both plasmas. The peak $m/z = 31$ (attributed to

16128869, 2024, 12, Downloaded from https://onlinelibrary.wiley.com/doi/10.1002/ppap.202400166 by Bibliothecaire En Chef Uni Catholique De Louvain (Ucl), Wiley Online Library on [27/01/2025]. See the Terms and Conditions (https://onlinelibrary.wiley.com/terms-and-conditions) on Wiley Online Library for rules of use; OA articles are governed by the applicable Creative Commons License

TABLE 4 | Attribution of the various peaks observed by mass spectrometry measurement of propanol-based plasma (left) and allyl alcohol-based plasma (right). $(M–xH)^+$ represents the corresponding precursor with x hydrogen atoms missing.

Propanol peak attributions		Allyl alcohol peak attributions	
m/z	**Ions**	***m/z***	**Ions**
2	H_2^+	18	H_2O^+
15–16	$CH_{3\text{-}4}^+$	26–29	$C_2H_{2\text{-}5}^+$; CO^+
25–30	$C_2H_{1\text{-}6}^+$; CO^+	39–44	$C_3H_{3\text{-}8}^+$
29–31	$H_{1\text{-}3}CO^+$	40–45	$C_2H_{0\text{-}5}O^+$
39–44	$C_3H_{3\text{-}8}^+$	44	CO_2^+
44	CO_2^+	57	$(M\text{-}H)^+$
40-45	$H_{0\text{-}5}C_2O^+$		
56–58	$(M\text{-}2H)^+$; $(M\text{-}3H)^+$; $(M\text{-}4H)^+$		

H_3CO^+) shows a high intensity for the propanol plasma and is likely produced by the breakage of a C–C bond in the precursor. H_2O peak is significantly more intense in the propanol plasma than in the allyl alcohol plasma. The extremely high intensity of H and H_2 could indicate plasma surface recombination. The formation of both hydrogen and water will be discussed later. It should be noted that sometimes, the discrimination between hydrocarbon peaks and fragments containing the heteroelement can be difficult due to isobaric interferences (e.g., $m/z = 44$ for $C_3H_8^+$; CO_2^+ and $C_2H_4O^+$ or $m/z = 28$ for $C_2H_4^+$ and CO^+). Consequently, several peaks in the mass spectra can be attributed to more than one fragment, as presented in Table 4.

It is worth noting that stable oxygen-based molecules (i.e., H_2O, CO_2 at $m/z = 18$ and 42, respectively) are produced in both plasmas. Their production limits the amount of oxygen available to be incorporated into the PPF. In order to validate this hypothesis, the relative intensity of H_2O in propanol and allyl alcohol plasmas has been evaluated and compared (Figure 11).

The relative intensity of H_2O in propanol discharge is almost two times higher than that in allyl alcohol one (i.e., 12 vs. 7.5, respectively), which can thus explain the lower oxygen content in these PPFs. Note that the relative proportion of CO_2 cannot be properly evaluated owing to isobaric interference with $C_2H_4O^+$ and $C_3H_8^+$ ($m/z = 44$) fragments. It should be mentioned that the presence of CO_2 would also indicate a strong etching process, although this cannot be confirmed from the available data.

3.2 | Discussion

Based on all the results collected, the chemical nature of the precursor has been unambiguously identified as a critical parameter in the growth mechanism of PPFs as a function of T_S. Although the physicochemical properties of allyl-PPF are dramatically affected by T_S, propanol-based PPFs are impacted to a much lower extent. Aiming at understanding these differences, the evolution of the deposition rates (R) as a function of T_S for

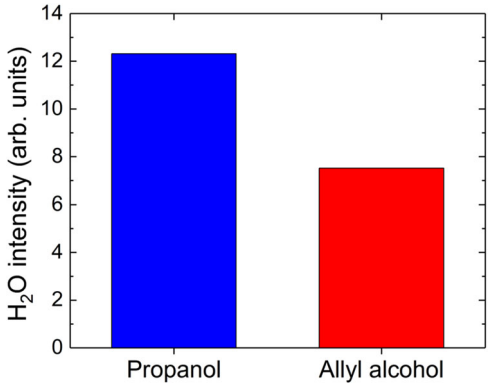

FIGURE 11 | Relative intensity of H_2O peaks in the mass spectra of propanol (blue) and allyl alcohol (red) plasmas, respectively.

both PPF families was measured. Indeed, it was shown in the literature that investigating the deposition kinetics versus the experimental conditions can provide crucial information about the growth mechanism of the layers [47, 71, 72].

Figure 12a shows that, for both PPF families, R decreases with T_S (i.e., from 2.07 ± 0.07 to 0.57 ± 0.01 nm/min for prop-PPF and from 28.3 ± 0.6 to 5.02 ± 0.23 nm/min for allyl-PPF) following an exponential law (red lines on Figure 12a), in accordance with the results observed in the literature for different PPF families [33, 34]. Interestingly, R is not only higher regardless of T_S but also varies in a wider range for allyl-PPF, which shows a greater variety of mechanical behaviors (i.e., from high-viscosity liquids to elastic solids). This suggests a correlation between the physicochemical properties of PPFs and their deposition rates.

In order to understand these observations, some basic principles of the molecular growth mechanism of PPFs need to be described. Reactive species (mainly radicals and to a lesser extent ions) are created in the plasma by electronic collisions. At the same time, the growing film is continuously bombarded by positive ions (with a kinetic energy typically ranging from 10 to 30 eV), inducing breakage of chemical bonds at the interface, and thus the formation of surface radical sites [70, 73]. Therefore, the film-forming species produced in the plasma adsorb at the interface and react with the surface-activated sites through the formation of a chemical bond, as considered in the Activated Growth Model ("AGM") developed by d'Agostino in the 1980s [2, 23].

Based on this approach, R is proportional to the flux of film-forming species toward the interface (F_R) and the density of surface reactive sites (S_R):

$$R \sim F_R . S_R, \tag{4}$$

For a more in-depth understanding of the interaction of the film-forming species with the interface, it can be considered that, at first, the reactive moieties are physisorbed in a "weakly adsorbed state" [72]. Then, they diffuse on the surface, before reaching a surface radical to form a chemical bond through a recombination reaction or the opening of a double or triple bond if the adsorbed species is, for example, an allyl alcohol or

16128869, 2024, 12, Downloaded from https://onlinelibrary.wiley.com/doi/10.1002/ppap.202400166 by Bibliothecaire En Chef Uni Catholique De Louvain (Ucl), Wiley Online Library on [27/01/2025]. See the Terms and Conditions (https://onlinelibrary.wiley.com/terms-and-conditions) on Wiley Online Library for rules of use; OA articles are governed by the applicable Creative Commons License

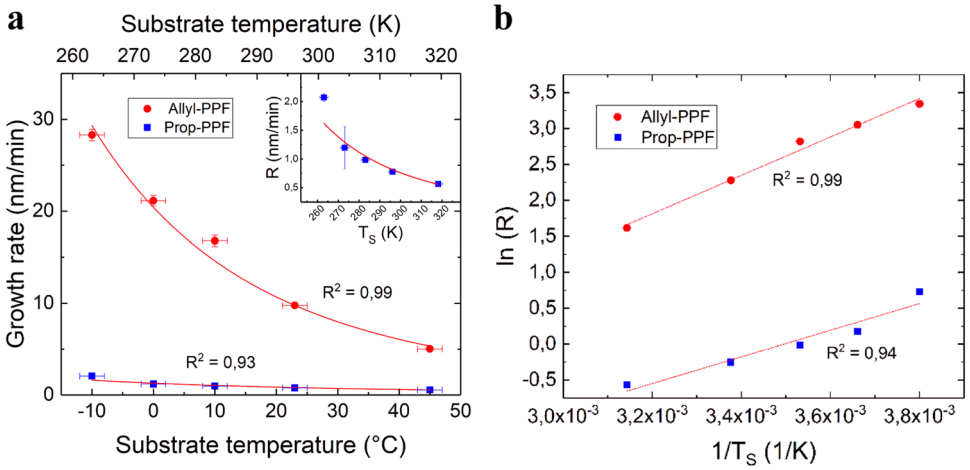

FIGURE 12 | (a) Growth rate of allyl-PPF (red) and prop-PPF (blue) as a function of the substrate temperature. Red lines show exponential laws fitted to each PPF family. The inset shows the growth rate of prop-PPF in more detail. (b) Evolution of Ln (R) as a function of inverse T_S for propanol (blue) and allyl alcohol (red). The red lines show the linear fittings of each precursor.

acetylene molecule [72]. Considering this mechanism, the residence time (τ), in other words the mean time that the particles spend on a surface before desorption, is crucial for the chemical incorporation of the film-forming species. Indeed, increasing (decreasing) τ results in a higher (lower) probability for the reactive specie to find a chemisorption site before being desorbed. Considering this statement, Equation (4) can be rewritten as:

$$R \sim F_R . S_R . \tau. \quad (5)$$

Actually, τ is defined according to the following equation [74]:

$$\tau = \tau_o e^{\frac{-E_{phys}}{k_B T_S}}, \quad (6)$$

where τ_0, $E_{phys,}$ and k_B correspond to the smallest possible residence time (i.e., the inverse of the vibrational frequency of the surface bond, ~10^{-12}–10^{-13} s), the physisorption energy, and the Boltzmann constant, respectively.

Then, insertion of Equations (5) into (6) yields

$$R \sim F_R . S_R . \tau_o e^{\frac{-E_{phys}}{k_B T_S}}. \quad (7)$$

From the above equation, is understood that only the exponential term depends on T_S, explaining the trend observed in Figure 12a regarding R. However, F_R and S_R directly depend on the fragmentation degree of the precursor in the plasma (α) and on the energy of the bombarding ions, respectively. A similar equation successfully described R dependency on T_S for propanethiol and propylamine plasma polymerization [47].

Plotting ln (R) as a function of $1/T_s$ yields E_{phys} (see Figure 12b): $E_{phys} = -0.14 \pm 0.02$ eV for prop-PPF and -0.23 ± 0.01 eV for allyl-PPF. These are typical physisorption values of adsorbed species on a given surface [75–77]. E_{phys} can be considered as an apparent physisorption energy of the film-forming species when in a weakly adsorbed state. It should be highlighted that the nearly constant chemical composition of both oxygen-based PPF families suggests that E_{phys} values of pure hydrocarbon-based film-forming species and the ones containing the heteroelement are close.

The E_{phys} value measured for allyl-PPF is significantly higher than that for prop-PPF. This supports differences from a chemical point of view in the flux of species contributing to the layer growth, as already suggested by the mass spectrometry analysis (Figure 9a–f and Table 4). Notably, allyl alcohol spectra present a $(M–H)^+$ peak at m/z 57, corresponding to a radical with a double bond. Interestingly, previous studies have found that unsaturated radicals presented a higher sticking coefficient [78]. Consequently, it can reasonably be expected that this radical would significantly contribute to the film growth, explaining the higher growth rate and E_{phys} of allyl-PPF. It should be noted that the presence of $(M–H)^+$ in allyl alcohol plasma might also contribute to the higher oxygen concentration of allyl-PPF, as this fragment contains 25% oxygen. Meanwhile, prop-PPF is formed by the reaction of saturated species with a lower sticking coefficient, leading to an unselective process and a lower growth rate and E_{phys}. The large production of hydrogen and dihydrogen in propanol plasma might also contribute to this slower deposition rate by etching the coating during its formation. As already mentioned, a reduced oxygen content in prop-PPF could also originate from higher formation of oxygen-containing unreactive species such as water.

However, the higher R of allyl alcohol cannot totally be explained by a different flux of growing species associated with a higher E_{phys}. Indeed, in a previous study using identical conditions, propylamine-based PPF showed an E_{phys} similar to allyl-PPF synthesized in identical conditions despite the significantly lower deposition kinetics shown by the former (i.e., R quite close to that of prop-PPF) [47]. Considering Equation (7), another factor must be considered, that is, F_R. In a first approach, F_R can be assimilated to α of the precursor. Indeed, the more the precursor is fragmented, the more film-forming species are created in the discharge. As shown in Figure 10, α is the highest for allyl alcohol (i.e., ~0.76) contributing to its highest R in comparison with propanol in the studied

16128869, 2024, 12, Downloaded from https://onlinelibrary.wiley.com/doi/10.1002/ppap.202400166 by Bibliothecaire En Chef Uni Catholique De Louvain (Ucl), Wiley Online Library on [27/01/2025]. See the Terms and Conditions (https://onlinelibrary.wiley.com/terms-and-conditions) on Wiley Online Library for rules of use; OA articles are governed by the applicable Creative Commons License

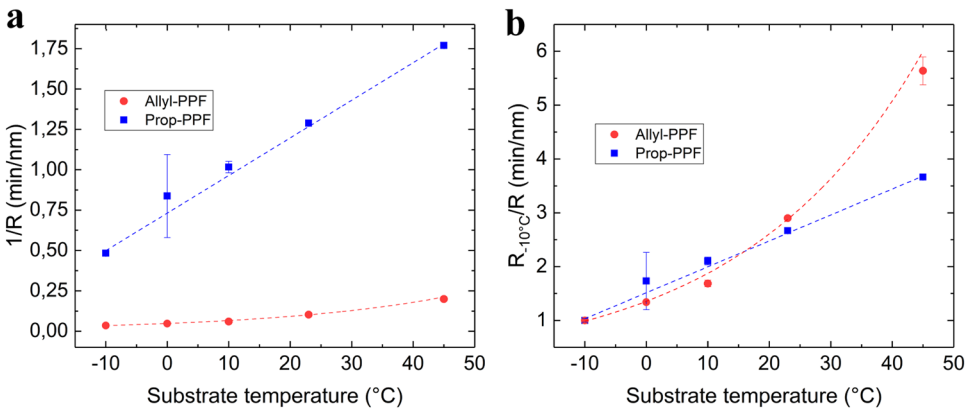

FIGURE 13 | (a) Evolution of $1/R$ for each PPF family as a function of T_S. (b) Evolution of $1/R$ normalized according to $1/R$ at $T_S = -10°C$ for each PPF family as a function of T_S. The dashed lines in (a) and (b) represent the exponential character of the evolution for each PPF family.

experimental conditions. Similarly, the comparable R for prop-PPF from this work and propylamine-based PPF reported from a previous study [47] could be explained by the balance between the exponential term and α. Although the propylamine-based PPF presents a higher E_{phys} (i.e., -0.25 ± 0.03 eV), α could be expected to be higher for prop-PPF. These two parameters would thus counterbalance each other, leading to close deposition kinetics.

From Equation (7) is clear that the density of surface reactive sites, hardly accessible experimentally, can also affect R. The latter is related to the ionic bombardment (and the UV radiation) that continuously activates the surface during the PPF growth [70, 73]. As the energy at the growing film interface is mainly influenced by the plasma parameters (i.e., electron density and electron temperature), it can thus be reasonably assumed that, in our experimental conditions, S_R should be similar regardless of the precursor.

Interestingly, it is also important to mention that, for a given PPF family, investigation of R versus T_S enables quantitative determination of important quantities regarding the plasma surface interaction (e.g., E_{phys}). This approach would be complementary to the macroscopic one developed by Hegemann enabling determination of the activation energy of several precursors regarding their dissociation in the plasma by studying R as a function of the energy invested per particle [71]. Combined use of both methods would yield a more complete view of the plasma polymerization process.

At this stage, it has been observed that the evolution of T_T and, hence, the mechanical properties of PPF arise from the evolution of χ as a function of T_S. On the other hand, R varies as a function of T_S and strongly depends on the precursor. Interestingly, the highest R is observed for PPF with a liquid behavior (i.e., allyl-PPF synthesized at $T_S \leq 10°C$), whereas the lowest R corresponds to hard elastic PPF (i.e., prop-PPF synthesized at any T_S, allyl-PPF at $T_S = 45°C$), suggesting a correlation between these properties. In order to understand this observation, the concept of energy density (ε) must be considered. This parameter can be defined as the energy brought to the growing film through ionic bombardment and normalized with respect to the total amount of matter deposited according to [26, 79]:

$$\varepsilon = \frac{\Gamma_i E_{mean}}{R}, \tag{8}$$

where Γ_i corresponds to the flux of ions reaching the growing film and E_{mean} is the mean energy of the bombarding ions. For several PPF families, a linear correlation has been found between χ (directly influencing the mechanical properties and T_T) and ε [79].

As in this experimental window, only T_S is varied, it can be rationally assumed that Γ_i and E_{mean} (as mentioned above, mainly influenced by the plasma parameters, that is, electron density and electron temperature) are identically irrespective of the precursor. On the other hand, as previously shown, R is highly sensitive toward the precursor and T_S. For both PPF families, according to Equation (8), ε increases with T_S (as R decreases). Therefore, this explains the increase in χ, which affects the mobility of the molecular segments and hence T_T of the material. From Figure 13a, it can be observed that the highest $1/R$ (hence ε) are obtained for prop-PPF, which shows an elastic behavior. Intermediate $1/R$ values (i.e., below 0.5 but higher than 0.05 min/nm) correspond to allyl-$PPF_{45°C}$ and allyl-$PPF_{23°C}$ showing viscoelastic properties, whereas the lowest $1/R$ values (i.e., ≤ 0.05 min/nm) characterize liquid PPF (allyl-PPF synthetized at $T_S \leq 10°C$).

Combining Equations (7) and (8) yields

$$\varepsilon \sim \frac{\Gamma_i E_{mean}}{F_R . S_R . \tau_0 e^{\frac{-E_{phys}}{k_B T_S}}}, \tag{9}$$

It can be estimated that ε increases by a factor of 4 and 6 for prop-PPF and allyl-PPF as a function of T_S, respectively (see Figure 13b). The larger variation in terms of energy density for allyl alcohol results from its higher E_{phys} (Equation 9). This could explain the more pronounced impact of T_S on χ and hence on the mechanical behavior of this PPF. Indeed, progressively increasing T_S for allyl-PPF results in a liquid coating for $T_S \leq 10°C$, then a viscoelastic material at $T_S = 23°C$, and finally an elastic solid at $T_S = 45°C$. If the fluid nature of PPF arises from high R values, the evolution of the mechanical properties is mainly determined by E_{phys}. For propanol-based PPF, the lower R (i.e., higher ε)

16128869, 2024, 12, Downloaded from https://onlinelibrary.wiley.com/doi/10.1002/ppap.202400166 by Bibliothecaire En Chef Uni Catholique De Louvain (Ucl), Wiley Online Library on [27/01/2025]. See the Terms and Conditions (https://onlinelibrary.wiley.com/terms-and-conditions) on Wiley Online Library for rules of use; OA articles are governed by the applicable Creative Commons License

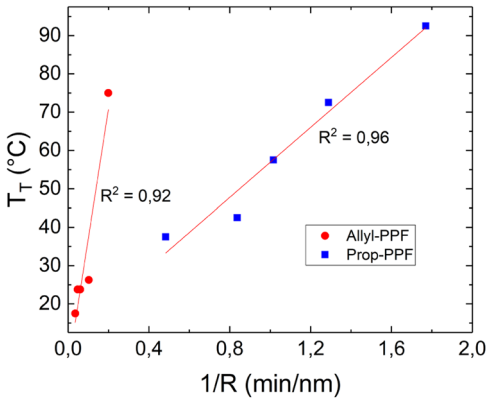

FIGURE 14 | Evolution of T_T as a function of the inverse of R for prop-PPF (blue) and allyl-PPF (red). The red lines show the linear fitting of each precursor.

gives rise for all T_S to a χ high enough for the PPF to behave as a hard elastic solid.

To rationalize these data, the evolution of T_T is plotted as a function of $1/R$ (i.e., proportional to ε_{surf} in our experimental window). As can be observed in Figure 14, for both PPF families, T_T is linearly correlated to $1/R$ and hence ε_{surf}, validating our hypothesis. Interestingly, the evolution of T_T for allyl-PPF as a function of $1/R$ reveals a more important impact of ε_{surf} for this precursor, highlighting the importance of the unsaturation degree of the precursor in the growth mechanism of PPF.

4 | Conclusion

This study explores how the substrate temperature affects the mechanical properties of plasma polymers and their link with their glass transition, using allyl alcohol and propanol as precursors differing from their hydrocarbon skeleton (i.e., saturated for propanol and unsaturated for allyl alcohol). The objective was to comprehend the relationship between mechanical properties and the mechanisms governing the layer formation to identify the main phenomena influencing the glass transition and consequently the mechanical properties of the plasma polymer.

Although the mechanical properties of propanol-based plasma polymers remain unaffected by the thermal conditions of the substrate (i.e., elastic solid with a modulus of 4 GPa), the substrate temperature markedly influences the mechanical behavior of allyl-PPF undergoing a transition from a highly viscous liquid (with viscosity ranging from ~10 to ~10^2 Pa.s) to a hard elastic solid (with a modulus of 3.7 GPa) for T_S increasing from −10°C to 45°C. These findings were correlated with the evolution of the surface transition temperature associated with the glass transition of the material. For a given precursor, it was observed that T_T is not affected by the chemical composition of the PPF, but rather by the cross-linking density of the layers. The latter is governed by the energy density of bombarding ions on the growing film (correlated with the inverse of the deposition rate). For allyl-PPF, higher R values result in low cross-linking density reducing the glass transition below the room temperature, thus explaining the observed liquid behavior for $T_S \leq 10$°C. Conversely, lower deposition rates for prop-PPF give rise to a polymeric network with higher cross-linking density and thus a glass transition above the room temperature, explaining why the material behaves as a hard elastic solid regardless of Ts. The difference in the deposition kinetics arises from the different fragmentation degree of the precursor (76% for allyl alcohol vs. 53% for propanol) and the apparent physisorption energy of the film-forming species (−0.23 vs. −0.14 eV for allyl alcohol and propanol, respectively).

For allyl alcohol, the larger control offered by T_S on the mechanical properties of PPFs in comparison to other synthesis parameters can be attributed to the exponential dependence of ε with T_S combined with a high E_{phys}. Indeed, considering the most investigated tuning parameter, namely, the power dissipated into the discharge, the deposition rate and the flux of bombarding ions evolve in the same way, resulting in a lower variation of ε and, hence, mechanical properties of the layers. Nevertheless, in contrast to T_S, the energy load in the plasma has been identified as an important synthesis parameter to tailor the surface chemical composition of the PPF. Therefore, both the power and the substrate temperature could be combined to modulate the surface composition and the mechanical properties of PPFs, offering additional degree of freedom for material optimization. Based on these considerations, it is obvious that the substrate temperature should now be considered as an additional experimental parameter that can improve the physicochemical properties of PPFs, paving the way for their wider use in practical applications. For the sake of completeness, it has also been shown that investigating the deposition kinetics versus T_S provides valuable information regarding the plasma/surface interaction, which can improve the fundamental understanding of the growth of the layer at the molecular level.

Acknowledgments

This publication was supported by the French Community of Belgium ("Communauté française de Belgique") through a FRIA grant.

Conflicts of Interest

The authors declare no conflicts of interest.

Data Availability Statement

The data that support the findings of this study are available on request from the corresponding author. The data are not publicly available due to privacy or ethical restrictions.

References

1. N. Inagaki, *Plasma Surface Modification and Plasma Polymerization* (Boca Raton: CRC Press Inc, 1996).

2. H. Biederman, *Plasma Polymer Films* (London: Imperial College Press, 2004).

3. L. M. Han, R. B. Timmons, and W. W. Lee, "Pulsed Plasma Polymerization of an Aromatic Perfluorocarbon Monomer: Formation of Low Dielectric Constant, High Thermal Stability Films," *Journal of Vacuum Science & Technology B: Microelectronics and Nanometer Structures Processing, Measurement, and Phenomena* 18 (2000): 799–804.

16128869, 2024, 12, Downloaded from https://onlinelibrary.wiley.com/doi/10.1002/ppap.202400166 by Bibliothecaire En Chef Uni Catholique De Louvain (Ucl), Wiley Online Library on [27/01/2025]. See the Terms and Conditions (https://onlinelibrary.wiley.com/terms-and-conditions) on Wiley Online Library for rules of use; OA articles are governed by the applicable Creative Commons License

4. H. Kobayashi, A. T. Bell, and M. Shen, "Plasma Polymerization of Saturated and Unsaturated Hydrocarbons," *Macromolecules* 7 (1974): 277–283.

5. D. Thiry, N. Britun, S. Konstantinidis, et al., "Experimental and Theoretical Study of the Effect of the Inductive-to-Capacitive Transition in Propanethiol Plasma Polymer Chemistry," *Journal of Physical Chemistry C* 117 (2013): 9843–9851.

6. L. Denis, P. Marsal, Y. Olivier, et al., "Deposition of Functional Organic Thin Films by Pulsed Plasma Polymerization: A Joint Theoretical and Experimental Study," *Plasma Processes and Polymers* 7 (2010): 172–181.

7. A. Fahmy, R. Mix, A. Schönhals, and J. F. Friedrich, "Structure–Property Relationship of Thin Plasma Deposited Poly(Allyl Alcohol) Films," *Plasma Chemistry and Plasma Processing* 31 (2011): 477–498.

8. D. Thiry, M. Pouyanne, D. Cossement, A. Hemberg, and R. Snyders, "Surface Engineering of Bromine-Based Plasma Polymer Films: A Step Toward High Thiol Density Containing Organic Coatings," *Langmuir* 34 (2018): 7655–7662.

9. B. Joseph, N. Ninan, R. M. Visalakshan, et al., "Insights Into the Biomechanical Properties of Plasma Treated 3D Printed PCL Scaffolds Decorated With Gold Nanoparticles," *Composites Science and Technology* 202 (2021): 108544.

10. R. Förch, Z. Zhang, and W. Knoll, "Soft Plasma Treated Surfaces: Tailoring of Structure and Properties for Biomaterial Applications," *Plasma Processes and Polymers* 2 (2005): 351–372.

11. P. L. Girard-Lauriault, F. Truica-Marasescu, A. Petit, et al., "Adhesion of Human U937 Monocytes to Nitrogen-Rich Organic Thin Films: Novel Insights Into the Mechanism of Cellular Adhesion," *Macromolecular Bioscience* 9 (2009): 911–921.

12. E. Makhneva, A. Manakhov, P. Skládal, and L. Zajíčková, "Development of Effective QCM Biosensors by Cyclopropylamine Plasma Polymerization and Antibody Immobilization Using Cross-Linking Reactions," *Surface and Coatings Technology* 290 (2016): 116–123.

13. F. J. Vastola and J. P. Wightman, "The Rearrangement of Acetylene, Benzene, Ethane, Ethylene, Methane and Naphthalene in a Microwave Discharge," *Journal of Applied Chemistry* 14 (1964): 69–73.

14. A. R. Denaro, P. A. Owens, and A. Crawshaw, "Glow Discharge Polymerization—Styrene," *European Polymer Journal* 4 (1968): 93–106.

15. J. M. Tibbitt, R. Jensen, A. T. Bell, and M. Shen, "A Model for the Kinetics of Plasma Polymerization," *Macromolecules* 10 (1977): 647–653.

16. H. Yasuda, "Glow Discharge Polymerization," *Journal of Polymer Science: Macromolecular Reviews* 16 (1981): 199–293.

17. H. Yasuda, *Luminous Chemical Vapor Deposition and Interface Engineering* (Boca Raton: CRC Press, 2004).

18. J. Friedrich, "Mechanisms of Plasma Polymerization—Reviewed From a Chemical Point of View," *Plasma Processes and Polymers* 8 (2011): 783–802.

19. H. Yasuda and T. Yasuda, "The Competitive Ablation and Polymerization (CAP) Principle and the Plasma Sensitivity of Elements in Plasma Polymerization and Treatment," *Journal of Polymer Science Part A: Polymer Chemistry* 38 (2000): 943–953.

20. A. R. Westwood, "Glow Discharge Polymerization—I. Rates and Mechanisms of Polymer Formation," *European Polymer Journal* 7 (1971): 363–375.

21. H.-U. Poll, M. Arzt, and K.-H. Wickleder, "Reaction Kinetics in the Polymerization of Thin Films on the Electrodes of a Glow-Discharge Gap," *European Polymer Journal* 12 (1976): 505–512.

22. R. d'Agostino, F. Cramarossa, and S. De Benedictis, "Chemical Mechanisms in C_3F_8-H_2 Radiofrequency Discharges," *Plasma Chemistry and Plasma Processing* 4 (1984): 21–31.

23. R. D'Agostino, F. Cramarossa, F. Fracassi, et al., "Polymer Film Formation in C_2F_6 H_2 Discharges," *Thin Solid Films* 143 (1986): 163–175.

24. A. J. Beck, S. Candan, R. D. Short, A. Goodyear, and N. S. J. Braithwaite, "The Role of Ions in the Plasma Polymerization of Allylamine," *The Journal of Physical Chemistry B* 105 (2001): 5730–5736.

25. A. Michelmore, J. D. Whittle, and R. D. Short, "The Importance of Ions in Low Pressure PECVD Plasmas," *Frontiers in Physics* 3 (2015): 3.

26. D. Hegemann, U. Schütz, and E. Körner, "Macroscopic Approach to Plasma Polymerization Using the Concept of Energy Density," *Plasma Processes and Polymers* 8 (2011): 689–694.

27. D. T. Clark and A. Dilks, "ESCA Applied to Polymers. XVIII. RF Glow Discharge Modification of Polymers In Helium, Neon, Argon, and Krypton," *Journal of Polymer Science: Polymer Chemistry Edition* 16 (1978): 911–936.

28. M. Hudis, "Surface Crosslinking of Polyethylene Using a Hydrogen Glow Discharge," *Journal of Applied Polymer Science* 16 (1972): 2397–2415.

29. M. R. Wertheimer, A. C. Fozza, and A. Holländer, "Industrial Processing of Polymers by Low-Pressure Plasmas: The Role of Vuv Radiation," *Nuclear Instruments and Methods in Physics Research Section B* 151 (1999): 65–75.

30. D. T. Clark and A. Dilks, "An Investigation of the Vacuum UV Spectra of Inductivity Coupled RF Plasmas Excited in Inert Gases as a Function of Some of the Operating Parameters," *Journal of Polymer Science: Polymer Chemistry Edition* 18 (1980): 1233–1246.

31. H. Yasuda and T. Hirotsu, "Critical Evaluation of Conditions of Plasma Polymerization," *Journal of Polymer Science: Polymer Chemistry Edition* 16 (1978): 743–759.

32. F. Fally, C. Doneux, J. Riga, and J. J. Verbist, "Quantification of the Functional Groups Present at the Surface of Plasma Polymers Deposited From Propylamine, Allylamine, and Propargylamine," *Journal of Applied Polymer Science* 56 (1995): 597–614.

33. T. B. Casserly and K. K. Gleason, "Effect of Substrate Temperature on the Plasma Polymerization of Poly(Methyl Methacrylate," *Chemical Vapor Deposition* 12 (2006): 59–66.

34. H. Yasuda and C. R. Wang, "Plasma Polymerization Investigated by the Substrate Temperature Dependence," *Journal of Polymer Science* 23 (1985): 87–106.

35. J. Petersen, J. Bardon, A. Dinia, D. Ruch, and N. Gherardi, "Organosilicon Coatings Deposited in Atmospheric Pressure Townsend Discharge for Gas Barrier Purpose: Effect of Substrate Temperature on Structure and Properties," *ACS Applied Materials & Interfaces* 4 (2012): 5872–5882.

36. H. K. Yasuda, "Some Important Aspects of Plasma Polymerization," *Plasma Processes and Polymers* 2 (2005): 293–304.

37. J. D. Whittle, R. D. Short, D. A. Steele, et al., "Variability in Plasma Polymerization Processes—An International Round-Robin Study," *Plasma Processes and Polymers* 10 (2013): 767–778.

38. R. Snyders, D. Hegemann, D. Thiry, O. Zabeida, J. Klemberg-Sapieha, and L. Martinu, "Foundations of Plasma Enhanced Chemical Vapor Deposition of Functional Coatings," *Plasma Sources Science and Technology* 32 (2023): 074001.

39. J. Ryssy, E. Prioste-Amaral, D. F. N. Assuncao, et al., "Chemical and Physical Processes in the Retention of Functional Groups in Plasma Polymers Studied by Plasma Phase Mass Spectroscopy," *Physical Chemistry Chemical Physics* 18 (2016): 4496–4504.

40. N. D. Leipzig and M. S. Shoichet, "The Effect of Substrate Stiffness on Adult Neural Stem Cell Behavior," *Biomaterials* 30 (2009): 6867–6878.

41. A. Michelmore, D. A. Steele, D. E. Robinson, J. D. Whittle, and R. D. Short, "The Link between Mechanisms of Deposition and the

16128869, 2024, 12, Downloaded from https://onlinelibrary.wiley.com/doi/10.1002/ppap.202400166 by Bibliothecaire En Chef Uni Catholique De Louvain (Ucl), Wiley Online Library on [27/01/2025]. See the Terms and Conditions (https://onlinelibrary.wiley.com/terms-and-conditions) on Wiley Online Library for rules of use; OA articles are governed by the applicable Creative Commons License

Physico-Chemical Properties of Plasma Polymer Films," *Soft Matter* 9 (2013): 6167.

42. J. Carneiro de Oliveira, A. Airoudj, P. Kunemann, F. Bally-Le Gall, and V. Roucoules, "Mechanical Properties of Plasma Polymer Films: a Review," *SN Applied Sciences* 3 (2021): 656.

43. S. Ligot, E. Bousser, D. Cossement, et al., "Correlation Between Mechanical Properties and Cross-Linking Degree of Ethyl Lactate Plasma Polymer Films," *Plasma Processes and Polymers* 12 (2015): 508–518.

44. D. Thiry, N. Vinx, P. Damman, et al., "The Wrinkling Concept Applied to Plasma-Deposited Polymer-Like Thin Films: A Promising Method for the Fabrication of Flexible Electrodes," *Plasma Processes and Polymers* 17 (2020): 2000119.

45. N. Vinx, P. Damman, P. Leclère, et al., "Investigating the Relationship Between the Mechanical Properties of Plasma Polymer-Like Thin Films and Their Glass Transition Temperature," *Soft Matter* 17 (2021): 10032–10041.

46. N. Vinx, D. Tromont, A. Chauvin, P. Leclère, R. Snyders, and D. Thiry, "Designing Nanostructured Organic-Based Material by Combining Plasma Polymerization and the Wrinkling Approach," *Langmuir* 39 (2023): 15231–15237.

47. N. Vinx, P. Leclère, C. Poleunis, et al., "The Influence of the Substrate Temperature on the Growth Mechanism of Amine- and Thiol-Based Plasma Polymers: A Comparative Study," *Plasma Processes and Polymers* (2023): 2300138.

48. L. Eriksson, E. Johansson, N. Kettaneth-Wold, et al., *Multi- and Megavariate Data Analysis Basic Principles and Applications*, 3rd ed. (Umeå: Umetrics Academy, 2006), 33–54.

49. D. Cossement, F. Renaux, D. Thiry, S. Ligot, R. Francq, and R. Snyders, "Chemical and Microstructural Characterizations of Plasma Polymer Films by Time-Of-Flight Secondary Ion Mass Spectrometry and Principal Component Analysis," *Applied Surface Science* 355 (2015): 842–848.

50. C. Poleunis, V. Cristaudo, and A. Delcorte, "Temperature Dependence of Arn+Cluster Backscattering From Polymer Surfaces: A New Method to Determine the Surface Glass Transition Temperature," *Journal of the American Society for Mass Spectrometry* 29 (2018): 4–7.

51. M. Chundak, C. Poleunis, V. Delmez, et al., "Argon Gas Cluster Fragmentation and Scattering as a Probe of the Surface Physics of Thermoset Polymers," *Applied Surface Science* 533 (2020): 147473.

52. P. Trtik, J. Kaufmann, and U. Volz, "On the Use of Peak-Force Tapping Atomic Force Microscopy for Quantification of the Local Elastic Modulus in Hardened Cement Paste," *Cement and Concrete Research* 42 (2012): 215–221.

53. B. Pittenger, S. Osechinskiy, D. Yablon, and T. Mueller, "Nanoscale DMA With the Atomic Force Microscope: A New Method for Measuring Viscoelastic Properties of Nanostructured Polymer Materials," *JOM* 71 (2019): 3390–3398.

54. K. L. Johnson, K. Kendall, and A. D. Roberts, "Surface energy and the Contact of Elastic Solids," *Proceedings of the Royal Society of London. A. Mathematical and Physical Sciences* 324 (1971): 301–313.

55. A. Kwaśniewska, M. Świetlicki, A. Prószyński, and G. Gładyszewski, "The Quantitative Nanomechanical Mapping of Starch/Kaolin Film Surfaces by Peak Force AFM," *Polymers* 13 (2021): 244.

56. B. Pittenger, N. Erina and C. Su, "Mechanical Property Mapping at the Nanoscale Using PeakForce QNM Scanning Probe Technique," in *Nanomechanical Analysis of High Performance Materials*, ed. A. Tiwari (Dordrecht: Springer Netherlands, 2014), 31–51.

57. H.-J. Butt, B. Cappella, and M. Kappl, "Force Measurements With the Atomic Force Microscope: Technique, Interpretation and Applications," *Surface Science Reports* 59 (2005): 1–152.

58. J. Bicerano, "Glass Transition," *Encyclopedia of Polymer Science and Technology* (Hoboken, NJ: John Wiley & Sons, Inc., 2001), 655–677.

59. V. R. Gowariker, J. Sreedar and N. V. Viswanathan, *Polymer Science* (Halsted Press, 1986).

60. K. L. Ngai, "The glass transition and the glassy state," *Physical Properties of Polymers*. (Cambridge: Cambridge University Press, 2004), 72–152.

61. S. Candan, "Radio Frequency-Induced Plasma Polymerization of Allyl Alcohol and 1-Propanol," *Turkish Journal Chemistry* 26 (2002): 783–791.

62. M. B. Larsen, S.-J. Wang, and M. A. Hillmyer, "Poly(Allyl Alcohol) Homo- and Block Polymers by Postpolymerization Reduction of an Activated Polyacrylamide," *Journal of the American Chemical Society* 140 (2018): 11911–11915.

63. T. R. Gengenbach and H. J. Griesser, "Deposition Conditions Influence the Postdeposition Oxidation of Methyl Methacrylate Plasma Polymer Films," *Journal of Polymer Science Part A: Polymer Chemistry* 36 (1998): 985–1000.

64. A. P. Ameen, R. D. Short, and R. J. Ward, "The Formation of High Surface Concentrations of Hydroxyl Groups in the Plasma Polymerization of Allyl Alcohol," *Polymer* 35 (1994): 4382–4391.

65. S. Swaraj, U. Oran, A. Lippitz, J. F. Friedrich, and W. E. S. Unger, "Surface Analysis of Plasma-Deposited Polymer Films, 6," *Plasma Processes and Polymers* 2 (2005): 572–580.

66. L. Denis, D. Thiry, D. Cossement, et al., "Towards the Understanding of Plasma Polymer Film Behaviour in Ethanol: A Multi-Technique Investigation," *Progress in Organic Coatings* 70 (2011): 134–141.

67. D. Thiry, R. Francq, D. Cossement, M. Guillaume, J. Cornil, and R. Snyders, "A Detailed Description of the Chemistry of Thiol Supporting Plasma Polymer Films," *Plasma Processes and Polymers* 11 (2014): 606–615.

68. V. Cristaudo, D. Merche, C. Poleunis, et al., "Ex-Situ SIMS Characterization of Plasma-Deposited Polystyrene Near Atmospheric Pressure," *Applied Surface Science* 481 (2019): 1490–1502.

69. F. J. Aparicio, D. Thiry, P. Laha, and R. Snyders, "Wide Range Control of the Chemical Composition and Optical Properties of Propanethiol Plasma Polymer Films by Regulating the Deposition Temperature," *Plasma Processes and Polymers* 13 (2016): 814–822.

70. D. Thiry, S. Konstantinidis, J. Cornil, and R. Snyders, "Plasma Diagnostics for the Low-Pressure Plasma Polymerization Process: A Critical Review," *Thin Solid Films* 606 (2016): 19–44.

71. D. Hegemann, "Macroscopic Investigation of Reaction Rates Yielding Plasma Polymer Deposition," *Journal of Physics D: Applied Physics* 46 (2013): 205204.

72. A. Keudell, "Surface Processes During Thin-Film Growth," *Plasma Sources Science and Technology* 9 (2000): 455–467.

73. D. Thiry, F. Reniers, and R. Snyders, "A Joint Mechanistic Description of Plasma Polymers Synthesized at Low and Atmospheric Pressure," in *Surface Modification of Polymers*, eds. J. Pinson and D. Thiry (Weinheim, Germany: Wiley-VCH Verlag GmbH & Co. KGaA, 2019), 67–106.

74. D. Thiry, F. J. Aparicio, P. Laha, H. Terryn, and R. Snyders, "Surface Temperature: A Key Parameter to Control the Propanethiol Plasma Polymer Chemistry," *Journal of Vacuum Science & Technology A: Vacuum, Surfaces, and Films* 32 (2014): 050602.

75. B. A. De Moor, M.-F. Reyniers, and G. B. Marin, "Physisorption and Chemisorption of Alkanes and Alkenes in H-FAU: A Combined ab Initio–Statistical Thermodynamics Study," *Physical Chemistry Chemical Physics* 11 (2009): 2939.

76. A. S. Raman and A. Vojvodic, "Energy Trends in Adsorption at Surfaces," in *Handbook of Materials Modeling*, eds. A. Wanda and Y. Sidney (Cham: Springer International Publishing, 2020), 1321–1341.

16128869, 2024, 12, Downloaded from https://onlinelibrary.wiley.com/doi/10.1002/ppap.202400166 by Bibliothecaire En Chef Uni Catholique De Louvain (Ucl), Wiley Online Library on [27/01/2025]. See the Terms and Conditions (https://onlinelibrary.wiley.com/terms-and-conditions) on Wiley Online Library for rules of use; OA articles are governed by the applicable Creative Commons License

77. M. Scheffler and C. Stampfl, "Theory of Adsorption on Metal Substrates," in *Electronic Structure* (Elsevier Science, 2000), 285–356.

78. C. Hopf, T. Schwarz-Selinger, W. Jacob, and A. von Keudell, "Surface Loss Probabilities of Hydrocarbon Radicals on Amorphous Hydrogenated Carbon Film Surfaces," *Journal of Applied Physics* 87 (2000): 2719–2725.

79. D. Hegemann, E. Körner, N. Blanchard, M. Drabik, and S. Guimond, "Densification of Functional Plasma Polymers by Momentum Transfer During Film Growth," *Applied Physics Letters* 101 (2012): 211603.

Supporting Information

Additional supporting information can be found online in the Supporting Information section.

16128969, 2024, 12, Downloaded from https://onlinelibrary.wiley.com/doi/10.1002/ppap.202400166 by Bibliothecaire En Chef Uni Catholique De Louvain (Ucl), Wiley Online Library on [27/01/2025]. See the Terms and Conditions (https://onlinelibrary.wiley.com/terms-and-conditions) on Wiley Online Library for rules of use; OA articles are governed by the applicable Creative Commons License